Research Article | Vol. 30, No. 23 / 7 Nov 2022 / Optics Express 42678

Optics EXPRESS

High broadband light absorption in ultrathin MoS_2 homojunction solar cells

CARLOS BUENO-BLANCO, SIMON A. SVATEK, AND ELISA ANTOLIN*

Instituto de Energía Solar, Universidad Politécnica de Madrid, Avenida Complutense 30, 28040, Madrid, Spain
*elisa.antolin@upm.es

Abstract: Transition metal dichalcogenides (TMDCs) have been proposed as light absorber materials for ultrathin solar cells. These materials are characterized by their strong light-matter interaction and the possibility to be assembled into devices at room temperature. Here, we model the optical absorptance of an ultrathin MoS_2 absorber embedded in different designs of a 1D optical cavity. We find that up to 87% of the photons contained in the 300-700 nm range of the AM1.5G spectrum can be absorbed employing MoS_2 absorbers as thin as 10 nm sandwiched between a h-BN top layer and an optically thick Ag reflector. An h-BN/MoS_2/h-BN/Ag cavity produces 0.89 average absorptance for a 57-nm-thick MoS_2 slab and it also maximizes the absorption of extremely thin absorbers, between 1 and 9 nm. We also model a possible large-scale device on a glass substrate combined with indium-tin oxide (ITO) whose absorptance is comparable to the other presented structures. The high broadband absorption in these light-trapping structures is caused by the amplification of the zeroth Fabry-Perot interference mode. This study demonstrates that light absorption in ultrathin solar cells based on nanometric TMDC absorbers can compete with conventional photovoltaic technology and provides different simple optical designs to choose from depending on the electronic characteristics of the TMDC junction.

© 2022 Optica Publishing Group under the terms of the Optica Open Access Publishing Agreement

1. Introduction

Photovoltaic energy production is growing rapidly and the vast majority is based on the deployment of silicon solar cells, which have a relatively thick silicon absorbing layer (~ 150 µm). Alternatively, thin-film solar cells made of direct bandgap semiconductors such as III-V materials, CdTe, or CIGS allow for high efficiencies with lower absorber thickness between 1 and 4 µm [1]. However, this thickness reduction has not resulted yet in a decisive decrease of the fabrication cost with respect to silicon. Further thinning of photovoltaic devices would be desirable to reduce material consumption, to lower the economic and energetic cost of fabrication, and to produce low-weight and flexible devices that can expand the field of application of photovoltaics (building integrated, vehicle powering, wearable devices, etc.). However, a severe device thinning presents several challenges [2]. Conventional semiconductors can become transparent and fragile when reduced to extremely thin laminae, and their electronic properties become dominated by surface recombination. Various recent works present progress on these issues. Ultrathin GaAs devices with a 205-nm-thick absorber and 19.9% efficiency [3] or a 260-nm-thick absorber and 22.35% efficiency [4] have been reported (for comparison, the current record for thicker GaAs devices is 29.1%) [2]. These ultrathin devices rely on the use of sophisticated light trapping schemes, such as nanostructured mirrors or plasmonic grids. Following a different approach, Steenhoff *et al.* use an extremely thin (13 nm) absorber made of amorphous Ge to produce a solar cell that is compatible with low-cost fabrication and has an efficiency of almost 4% [5].

Recently, there has been great interest in transition metal dichalcogenides (TMDC) like MoS_2 as alternative absorber materials for ultrathin solar cells. These materials exhibit very strong light

#469931 https://doi.org/10.1364/OE.469931
Journal © 2022 Received 28 Jul 2022; revised 23 Sep 2022; accepted 24 Sep 2022; published 4 Nov 2022

Optics EXPRESS

absorption [6] and, as illustrated in Fig. 1(a), they could enable the transition from the 1 - 4 μm thickness range of conventional thin-film technologies to the < 100 nm thickness range, without applying complex light-trapping techniques. Figure 1(b) shows that the absorption coefficient of MoS_2 is significantly larger in the visible range (up to ~ 700 nm) than the coefficients of other semiconductors typically used in solar cells. Despite its relatively wide band gap energy, the large difference in absorption coefficient makes MoS_2 an interesting candite not only for a top cell in a tandem structure, but also for a single-gap device. Wide-gap TMDCs can be competitive for single-gap applications because in the ultrathin regime conventional semiconductors can only provide a limited photocurrent collection unless high-precision light-trapping structures are employed. We will show in this work that a 57-nm-thick MoS_2 absorber embedded in a simple layer structure can produce a single-gap photocurrent density of 18.2 mA/cm^2, whereas it has been reported that an 830-nm-thick silicon absorber in a nanophotonic architecture produces 19.7 mA/cm^2 [7]. Despite the much narrower bandgap of Si, the difference in photogeneration between the two ultrathin devices is small and it can be outweighed by other practical advantages of TMDCs. Notably, the layered crystalline structure of TMDCs allows the isolation of extremely thin laminae (down to the monolayer limit) with high chemical and mechanical stability and no dangling bonds on their surfaces (i.e., very reduced surface recombination). Due to the self-passivated nature of the laminae, devices can be made simply by putting them in physical contact at room temperature (van der Walls structures) and the deposition of nanosheets from solution is possible [8]. Another advantage of TMDCs is the reduction of material usage associated to the extreme device thinness. The potential increase in specific power (power produced per unit of mass) and the mechanical properties of the layered crystalline lattice make TMDCs particularly attractive for the industry of self-powered vehicles, particularly in space. Furthermore, Mo or W, are more abundant in the Earth crust than Cd, Te, or In, which are used in conventional thin-film approaches [9]. Therefore, layered TMDC semiconductors appear as natural candidates for the fabrication of ultrathin crystalline absorbers, possibly leading to lower costs (low temperature fabrication) and also opening the path to new photovoltaic applications as illustrated in Fig. 1(c).

Although the technology of TMDC-based solar cells is young, important experimental milestones have already been reached and it has been argued that efficiencies close to 20% are in reach in the next years [10]. Photodiodes at the ultimate thickness limit of two monolayers have been demonstrated with these materials (total absorber thickness ~1 nm) [11–14]. To increase light absorption and facilitate current transport, an intermediate thickness regime of several nanometers has been researched, reporting solar cells made of different combinations of MoS_2, $MoSe_2$, ReS_2, $ReSe_2$, WS_2, and WSe_2 [15–18] and recently an open circuit voltage of 1 V at a material bandgap of 1.3 eV has been achieved in a 120 nm thick MoS_2 homojunction [19]. This suggests that high efficiencies can be reached in a MoS_2 homojunction, and the question arises how to maximize light absorption with the minimum absorber thickness.

Different strategies to increase absorptance in TMDC-based devices have been proposed. For instance, an Al_2O_3 adlayer increases of the external quantum efficiency (EQE) of a WSe_2-based photodetector by 30% under monochromatic illumination (410 nm) [20]. The influence of a back metallic layer on the absorptance of photodetectors and solar cells made of thin layers of WSe_2, WS_2, and MoS_2 has also been reported with very high peak absorbances [16,21]. Also, the deposition of metallic nanoparticles has been reported to increase the EQE of TMDC absorbers to ~30% for monochromatic illumination [22]. However, for photovoltaic applications high broadband absorptance is required. The broadband absorptance at visible wavelengths has been shown to increase through the inclusion of monolayer TMDCs into photonic crystal nanocavities and averaged EQEs of the order of 50% across the visible spectrum have been achieved [22–24]. In this work we present h-BN-based cavity designs for ultrathin MoS_2 solar cells that maximize the total light absorption with respect to previously proposed architectures. The h-BN cavities

Optics EXPRESS

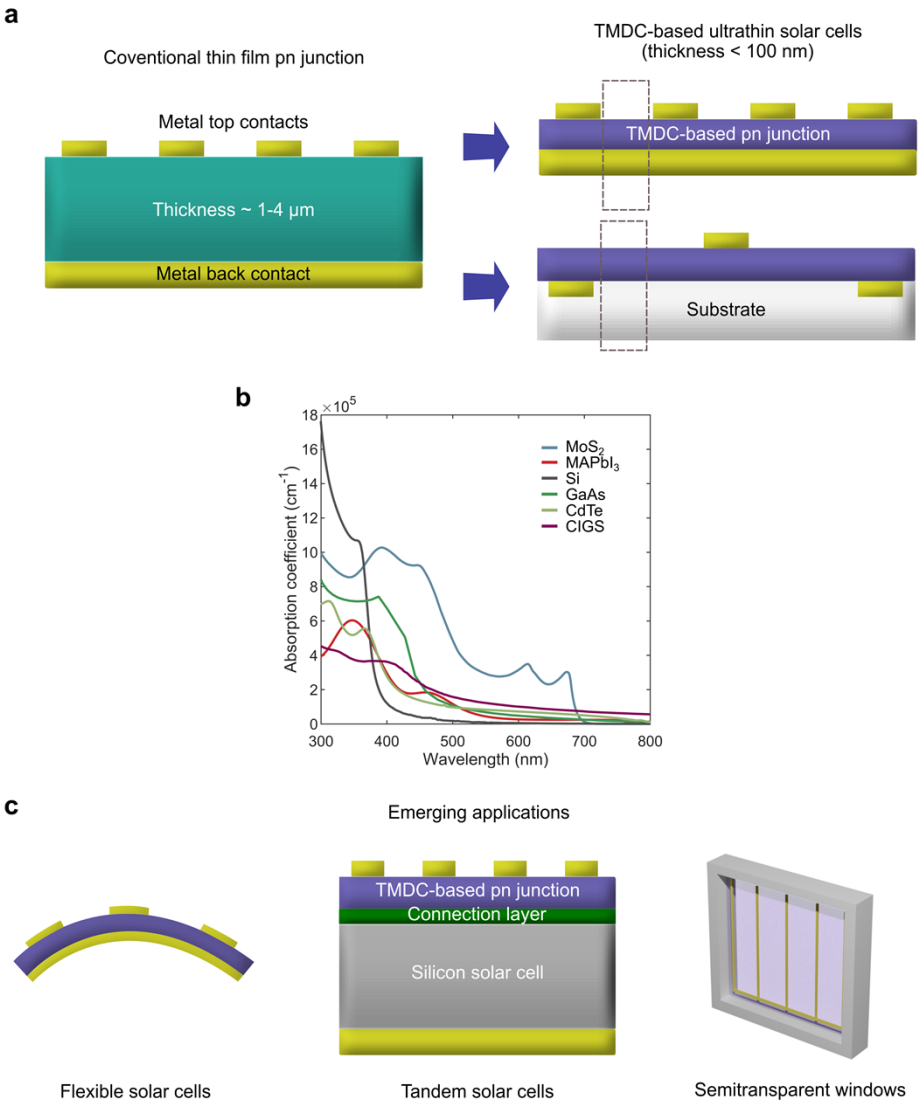

Fig. 1. (a) Illustration of the transition from thin-film to TMDC-based ultrathin technologies. (b) Absorption coefficient versus wavelength for different semiconductors typically used in solar cells. Values have been extracted from the following references: MoS_2 [26], $MAPbI_3$ [27], Si [28], GaAs [28], CdTe [29], and CIGS [30]. (c) Possible applications of TMDC-based devices beyond the conventional single-gap solar cell.

Optics EXPRESS

exploit interference effects and result in broadband averaged absorptances between 80% and 90% for a TMDC absorber thickness between 4 nm and ~100 nm. The designs are 1D and simple; they are compatible with large-scale fabrication and low-cost deposition techniques. They comprise a MoS_2 absorber, one or two h-BN layers, and a substrate (metallic or transparent). The high absorptance results from the amplification of the low-order absorption maxima in a resonant cavity, specially the zeroth order that appears in ultrathin highly absorbing media with suitable material boundaries, as described by Kats *et al.* [25].

2. Optical model

To model the TMDC-based ultrathin solar cells we consider a multilayer structure with homogeneous layers and plain and parallel interfaces. Such structures could be fabricated by spin-coating a solution of nanosheets and posterior annealing. This low-cost fabrication technique has proven to have very precise thickness control and homogeneity across 6" wafers for MoS_2 layers as thin as 2 nm [31]. A standard device design for a conventional pn junction and two possible TMDC-based ultrathin devices are shown in Fig. 1(a). In the standard solar cell, the junction is contacted from the top by a metal grid and from the bottom by a metal layer. For the ultrathin cells made of TMDCs it is possible to adopt the same architecture (design on the top) or to deposit the TMDC semiconductor onto an insulating material - which could have electrical and optical advantages - and use a metal grid also at the rear of the cell to extract the current (design on the bottom). This metal grid would be deposited on the substrate prior to the deposition of the semiconductor (it is not necessarily embedded in the substrate; it could simply be deposited on its surface). In our illustration we have located the top and rear metal fingers in alternating positions, which can be useful to avoid shunting in case the low-cost deposition of the absorber is not fully homogeneous, but this choice is not relevant for our results. We have modelled the two cases: metallic or dielectric substrate, also considering that the dielectric substrate can have a metallic layer underneath, not shown in the figure. For each case only the section surrounded by a dashed line has been simulated, not including metal grids.

With respect to the internal structure of the solar cell, we consider that the core is a MoS_2 pn homojunction [19]. It has been demonstrated that MoS_2 can be substitutionally doped to produce controlled n- and p-type layers [32] and, by placing one on top of another -even at room temperature – a homojunction can be formed. In contrast to conventional semiconductors, TMDCs have a very low surface recombination because of their layered crystalline lattice. Therefore, passivating layers (such as window and back surface field) are not required. Also, the van der Waals junction between a TMDC and a metal behaves can behave as an ohmic contact (if the metal is correctly chosen and the TMDC surface is not damaged). Therefore, intermetallic layers between the TMDC and the metal are, in principle, also not required. This lack of passivation and contact layers is one of the factors that make TMDCs extremely suitable for ultrathin devices. In our optical models, the whole solar cell is contained in a MoS_2 slab (containing an n and a p layer, whose thicknesses are relevant electronically, but not optically). Note that our results would not be directly applicable to a different MoS_2 solar cell structure (for example, one where a MoS_2 absorber is placed between to selective contacts).

The refractive indices (n) and extinction coefficients (k) of MoS_2 and h-BN have been taken from Refs. [26,33–36] and they are represented in the Supplementary Material, S1. As the optical properties of MoS_2 are not affected by the doping within the dopant concentration range of interest, we model the pn junction as a single MoS_2 slab and we use the refractive index of the pristine material. It is known that the n and k of monolayer and few-layer samples differ slightly from bulk values. It has been argued that the bulk properties are exactly reached when the sample has a thickness of 13 atomic layers in the case of MoS_2 (~ 8 nm) [37] or 8 atomic layers in the case of h-BN (~ 3 nm) [38]. However, there is a large scattering in the published n and k values for monolayer and few-layer MoS_2 [37,39,40]. The difference among published

Optics EXPRESS

monolayer values exceeds the difference between some of these values and the bulk values. In the case of h-BN, the optical properties of thicknesses between 2 monolayer and 7 atomic layers are not available in the literature. For this reason, we use bulk optical constants for all thicknesses.

In our model we consider normal incidence of sunlight on the top surface and calculate the variation of light flux within each layer following the method described by Centurioni [41]. This method uses the scattering-matrix method that allows to obtain the Poynting vector at every depth in the stack, which can be used to calculate variations in the photon energy flux within each layer. This yields the absorptance, reflectance and transmittance of every layer considering all internal reflections and interferences. We assume temporal coherence because the thickness of the MoS_2 slab is generally smaller than the coherence length of sunlight in that material and the thickness of transparent substrates is so large that no interference effects are observed in them using a coherent treatment. We assume spatial coherence as well, which is consistent with the smoothness of TMDC materials even if they are deposited from solution [31]. We quantify the broadband absorptance by averaging the wavelength-dependent absorptance in the range between 300 to 700 nm (more details below). This range is chosen considering the ultraviolet cut-off of the solar spectrum and the wavelength of the direct bandgap of MoS_2, which is 685 nm (see Supplementary Material, S11) [42].

3. Absorptance of a MoS_2 slab on a transparent substrate

We first calculate the absorptance of a slab of MoS_2 on a transparent substrate, see Fig. 2(a). We choose sapphire (Al_2O_3) as the substrate, but the results are generally applicable for transparent substrates with thickness of some hundreds of microns. When the calculations are repeated considering a glass substrate as a low-cost option, almost identical values are obtained if the condition of coherence is kept (see Supplementary Material, S2). Figure 2(b) shows absorptance spectra for several MoS_2 thicknesses. The features in this plot are difficult to interpret because interference maxima appear convoluted with excitonic absorption maxima (the extinction coefficient of MoS_2 presents two excitonic peaks at 620 and 680 nm). We find that for a thickness of only 60 nm the absorptance reaches values in the range of 0.5, profiting from an interference maximum at $\lambda \sim$580 nm. The interference effects are easier to identify in Fig. 2(c), where the average absorptance over the 300-700 nm range is plotted as a function of the absorber thickness.

We have used two definitions of average: the plain arithmetic average (blue curve), and the AM1.5G-weigthed average (orange curve), that is, the number of photons from the AM1.5G solar spectrum absorbed in the MoS_2 slab divided by the total number of photons available in the AM1.5G spectrum. The AM1.5G spectrum is an international standard for the global solar spectral irradiance received by a horizontal surface on the Earth. It is defined considering that sunrays have an optical path length that equals 1.5 times the thickness of the atmosphere. This standard is widely used in photovoltaics because it is close to the yearly average of solar irradiance for mid-latitudes. In our calculations, using the AM1.5G-weigthed average reflects the fact that there are fewer photons in the short-wavelength range of the spectrum than in the longer-wavelength range (see grey curve in Fig. 2(b)), and therefore, gives a more accurate estimation of the final photocurrent density in practical devices. When we present average absorptance values below, we always refer to the AM1.5G-weigthed average.

In Fig. 2(c) we find that the absorptance of a MoS_2 slab on sapphire tends towards a constant value ~0.5 at thicknesses above 100 nm, where transmission tends to zero and the other 50% of the light is loss to reflectance. By integrating the product of the absorptance and the AM1.5G spectrum we estimate that the MoS_2 slab can produce a maximum photocurrent density of 10.03 mA/cm^2. For lower thicknesses we find absorptance maxima at 8 nm, 66 nm, and 132 nm, which we label M0, M1 and M2, respectively. These peaks result from the constructive interference within the thin layer of multiple waves that have been reflected or refracted at the surfaces. This effect is usually called a Fabry-Perot (FP) interference. In the absence of a substrate, the FP

Optics EXPRESS

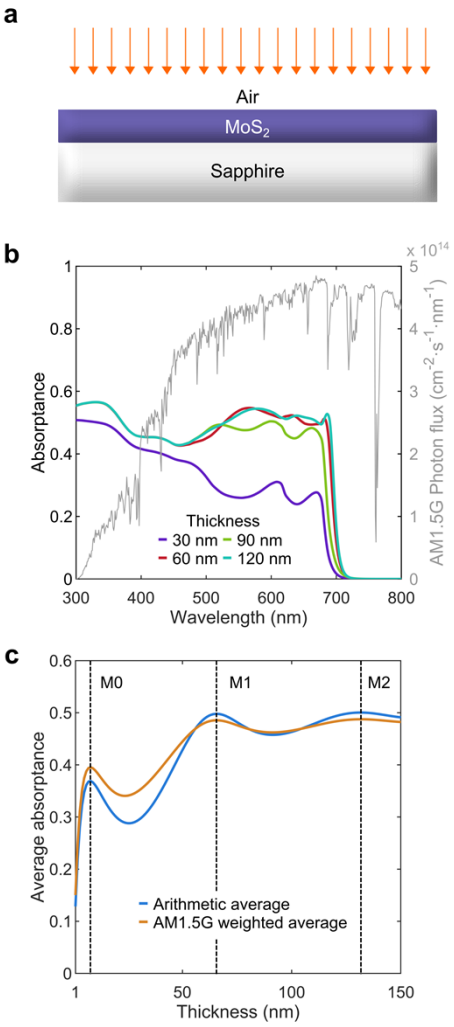

Fig. 2. (a) Schematic of the MoS_2/sapphire structure. (b) Absorptance for different MoS_2 thicknesses. (c) Comparison between average absorptance (blue) and weighted absorptance with AM1.5G spectrum (orange). Vertical dashed lines mark the interference maxima M0, M1, and M2.

Optics EXPRESS

maxima for a given wavelength λ appear at the resonant thicknesses d given by [43]

$$d = \mathrm{Re}\left(\frac{m\lambda}{2(n+ik)} - \frac{\lambda i}{2\pi(n+ik)} ln\left(\frac{n+ik+1}{n+ik-1}\right)\right) \quad (1)$$

where n is the refractive index and k the extinction coefficient of the material slab, and m (integer) is the interference order. Traditionally, FP interference has been mostly studied for transparent materials ($k \sim 0$), for which Eq. (1) can be approximated as $d \sim m\lambda/2n$. The slab of thickness d produces in that case a standing wave of half a wavelength because the phase shift of the wave reflected at the rear surface approaches 0. In the case of our MoS_2 slab, the absorption maximum M1 observed in Fig. 2(c) is the convolution of the FP maxima with order $m = 1$ calculated for all wavelengths in the AM1.5G spectrum. Similarly, M2 results from the FP maxima with order $m = 2$. The FP maxima in our slab are slightly shifted with respect to $d \sim m\lambda/2n$ because the extinction coefficient has a finite value (see Supplementary Material S3 for more details). On the other hand, the M0 maximum, which corresponds to $m = 0$, would not appear in a material with $k \sim 0$. The M0 maximum appears at a thickness much smaller than $\lambda/2n$. Note that, to have a resonance in such a small thickness, the phase shift of the waves reflected at the interfaces must have a non-trivial value (i.e., not 0 and not π, which are the trivial values for dielectrics with negligible absorption).

The phenomenon of zeroth order absorption it is of enormous interest for ultrathin photovoltaic devices, but has not been widely used yet. It has been described conceptually by Kats *et al.* [25] and Llorens *et al.* [43,44]. They have found that it can be very significant for materials with strong extinction coefficient and it can be amplified by the presence of a metallic layer under the semiconductor slab. For this purpose, the metal must have finite optical conductance, which allows the optimization of the reflection phase-shift at the interface [25].

4. Absorptance of 1D cavities containing h-BN

The following solar cell structures are designed to amplify the absorption maxima of Fig. 2(c) – especially M0 - in the MoS_2 absorber. Due to the high refractive index of MoS_2, in the structure of Fig. 2 half of the incident light is reflected. Therefore, it would be advantageous to deposit a material on top of the MoS_2 absorber that could act as anti-reflective layer. We have chosen h-BN because its refractive index approximately equals the geometric mean between the refractive indices of MoS_2 and air over a wide range of the visible spectrum (see Fig. 3) which makes it a good candidate for the optical coupling of these two media. Also, it is common practice to use h-BN in combination with TMDCs (and graphene) because h-BN also has a layered structure. When stacked onto each other, layered materials hold together by van der Waals forces which preserves the surface integrity on an atomic level, and the addition of h-BN layers to MoS_2 has proven to improve its electrical transport properties [45].

Figure 4(a) shows a solar cell structure containing a MoS_2 absorber on a sapphire substrate, covered by an h-BN layer, and Fig. 4(b) shows the AM1.5G-weighted average absorptance as a function of h-BN and MoS_2 thickness. We find indeed a notable improvement over the MoS_2/sapphire case for the absorption maxima M1 and M2. The maximum absorptance is 0.84, and the estimated maximum photocurrent density 17.20 mA/cm^2, found at M2 for 120 nm of MoS_2 and 56 nm of h-BN. This is an increase by 70% in comparison to bare MoS_2. Figure 2(c) shows the spectral absorptance for the two maxima M1 and M2. These results exceed the findings reported by Islam *et al.* [46] for MoS_2 absorbers under conventional antireflective coating materials (SiO_2, MgF_2, ...) which can be explained by the more suitable refractive index of h-BN. However, the zeroth FP mode has not been amplified as much in the h-BN/MoS_2/sapphire structure, as it is clearly observed in Fig. 4(g). The maximum absorptance values and optimal thicknesses for this and the following structures are compiled in Table 1.

Optics EXPRESS

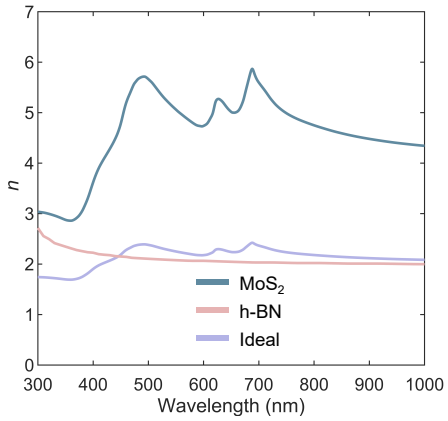

Fig. 3. Refractive index of MoS_2 (from Ref. [26]), h-BN (from Ref. [35]), and an ideal antireflective material for MoS_2 (geometrical mean of the refractive indices of MoS_2 and air).

Table 1. Optimum layer thicknesses, average absorptance (weighted over the 300 to 700 nm range of the AM1.G spectrum), and maximum photocurrent density under the AM1.5G spectrum for different MoS_2-based solar cell structures.

Structure	*Second top layer (nm)*	*Top layer (nm)*	*MoS_2 (nm)*	*Bottom layer (nm)*	*Absorptance*	*Max. photocurrent density (mA/cm^2)*
MoS_2/sapphire	-	-	8	-	0.40 (M0)	8.19
			66		0.49 (M1)	10.03
			132		0.49 (M2)	10.03
h-BN/MoS_2/sapphire	-	53	62	-	0.80 (M1)	16.38
		56	120		0.84 (M2)	17.2
h-BN/MoS_2/Ag		32	10	-	0.87 (M0)	17.81
		53	69		0.88 (M1)	18.01
h-BN/MoS_2/	-	46	37	-	0.86 (M1)	17.6
sapphire/Ag		54	98		0.87 (M2)	17.81
SiO_2/h-BN/	37	34	38	-	0.87 (M1)	17.81
MoS_2/sapphire/Ag	31	44	98		0.88 (M2)	18.01
h-BN/MoS_2/h-BN/Ag	-	31	10	1	0.87 (M0)	17.81
		52	57	48	0.89 (M1)	18.22
Glass/ITO/MoS_2/Ag	-	61	11	-	0.88 (M0)	18.01
		80	71		0.82 (M1)	16.79

Optics EXPRESS

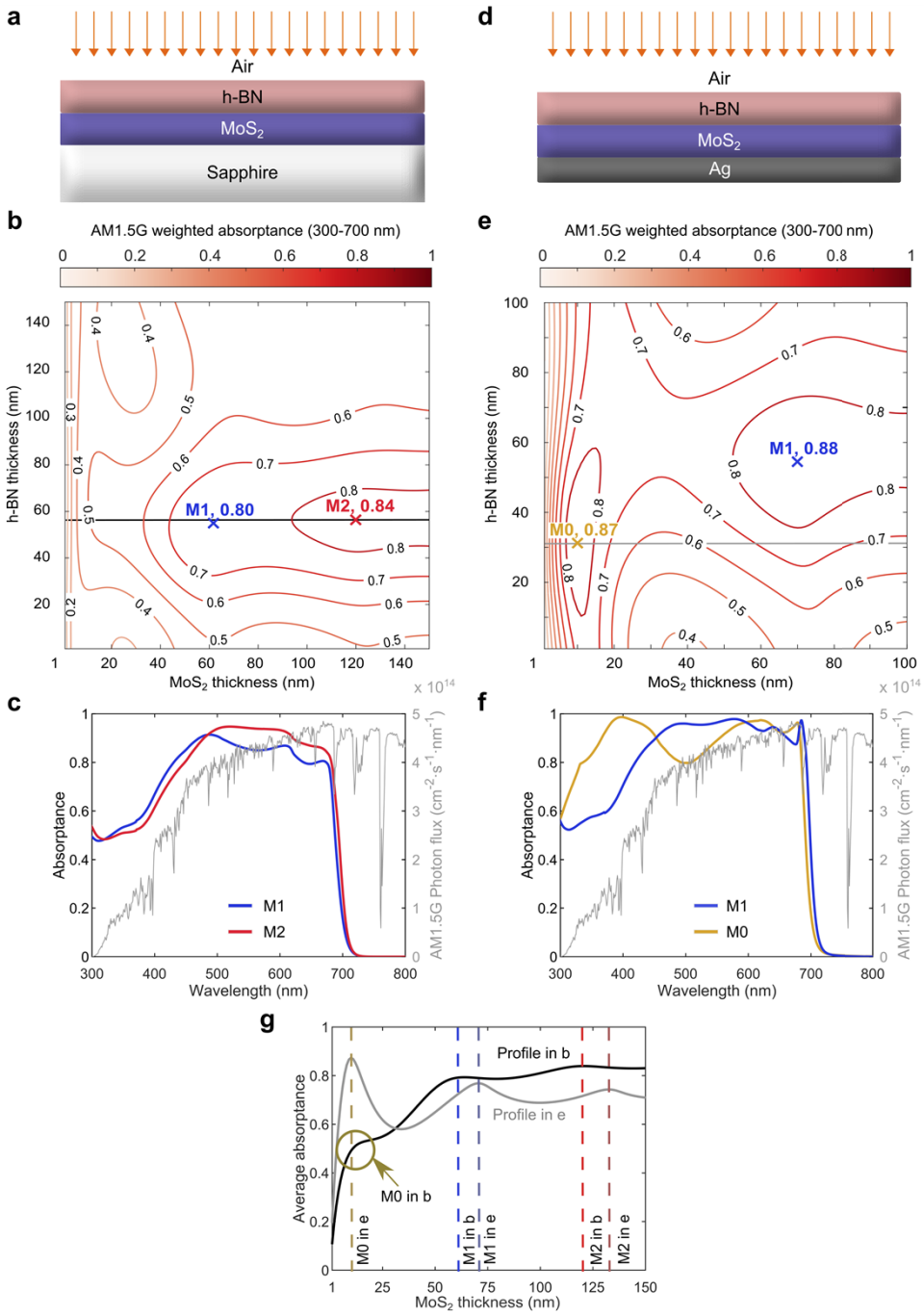

Fig. 4. (a) Schematic of h-BN/MoS_2/sapphire structure. (b) AM1.5G-weighted absorptance as a function of h-BN and MoS_2 thicknesses in the structure in (a). (c) Spectral absorptance for the optimal cases M1 (blue) and M2 (red). (d) Schematic of h-BN/MoS_2/Ag structure. (e) AM1.5G-weighted absorptance as a function of h-BN and MoS_2 thicknesses in the structure in (d). (f) Spectral absorptance for optimal cases of (e) M0 (yellow) and M1 (blue). (g) AM1.5G-weighted absorptance for a constant h-BN thickness and variable MoS_2 thickness extracted from the maps in (b) and (c). The black (grey) curve corresponds to the black (grey) horizontal line in map b (e). The optimum layer thicknesses and average absorptance for the curves in (c) and (f) can be found in Table 1.

Optics EXPRESS

The amplification of M0 requires a substrate material that produces an optimum phase-shift at the rear interface [25]. In Fig. 4(d) we present a structure with h-BN on the top and an optically thick Ag layer as substrate. Figure 4(e) shows the average absorption. The metal acts as a mirror, increasing the average absorption of M1 from 0.84 to 0.88, a most importantly, M0 is strongly amplified, reaching 0.87 for an extremely thin structure (MoS_2 10 nm, h-BN 32 nm). Integration with the AM1.5G spectrum yields a maximum photocurrent density of 18.01 mA/cm^2 for M2 and 17.81 mA/cm^2 for M1. Note that thinner absorbers are generally preferred in practical devices because the collection efficiency of photogenerated carriers decreases with thickness, although other factors such as lateral series resistance can make a design in the M1 thickness range desirable. Figure 4(f) shows the spectral absorbance of this structure at the M0 and M1 maxima. In the M0 case, the monochromatic absorptance at λ=399 nm is as high as 0.97, and if the device was used under an UV-rich spectrum, such as the AM0, the average absorption of the M0 structure would probably exceed that of the M1 structure. In Fig. 4(g) the amplification of the M0 mode in the h-BN/MoS_2/Ag architecture is very noticeable. We have modeled the same structure with an Al substrate as a low-cost alternative, see Supplementary Material S4. The result in that case is not as promising: M0 is only amplified to 0.77 absorptance and M1 reaches 0.85 In the case of Ag, reflection at the back interface is maximized due to the negligible refractive index of this material in the wavelength range above 350 nm. This condition is not met for Al. In Supplemental Materials section S12 there is more information about the effect of the complex index of refraction of the metal on the MoS_2 absorptance.

5. Absorptance of structures containing h-BN and back mirror

For some practical applications, a non-conductive substrate is desired, as shown in Fig. 1(a). In the next designs, we explore using a mirror at the back of the transparent sapphire substrate, as shown in Fig. 5(a). Figure 5(b) shows the average absorptance contour map. We find that the addition of the back mirror to the transparent substrate increases the absorptance with respect to the h-BN/MoS_2/sapphire case (Fig. 4 (a)-(c)) to reach 0.86 (M1) and 0.87 (M2) and it also shifts the optimum MoS_2 thickness to lower values: 37 (M1) and 98 nm (M2). We obtain a maximum photocurrent density of 17.81 mA/cm^2 for M2 and 17.60 mA/cm^2 for M1. However, the results are slightly worse than in the h-BN/MoS_2/Ag case (Fig. 4 (d)-(f)) and, most importantly, the M0 maximum is completely disappeared in this design. In this structure the reflected and transmitted components at the interfaces do not have the appropriated phase shift to generate a 2π total phase accumulation in a MoS_2 slab with thickness below $\lambda/4n$.

A possible route to enhance the performance of the h-BN/MoS_2/sapphire/Ag structure is to add a second antireflective layer to produce a graded refractive index transition. For this second layer the material choice is wider than for the first layer because it will not be deposited onto the absorber and has thus no degrading effect on the surface quality and electrical performance. Figure 5(d) shows a schematic of the solar cell structure containing a top SiO_2 antireflective layer and Fig. 5(e) shows the weighted absorptance for varying thicknesses of h-BN and MoS_2. The thickness of the SiO_2 layer has been optimized at each point of the map (see Supplementary Material S7). The results are virtually identical if MgF_2 is considered instead of SiO_2 (see Supplementary Material, S6). We find a slightly increased absorptance with respect to the single antireflective layer design: M1 reaches 0.87 and M2 reaches 0.88, equaling the performance of the h-BN/MoS_2/Ag stack. The spectral absorbance in Fig. 5(f) shows that the improvement comes from the UV-blue region. The addition of a second antireflective layer has a significant impact in that spectral range because the refractive index of h-BN does not couple optimally to the MoS_2 refractive index below $\lambda = 450$ nm (see Fig. 3). However, the AM1.5G spectrum has a low photon flux in the UV-blue region, which explains that the total averaged absorptance is not significantly enhanced. For space applications, where the spectrum has a greater UV contribution,

Optics EXPRESS

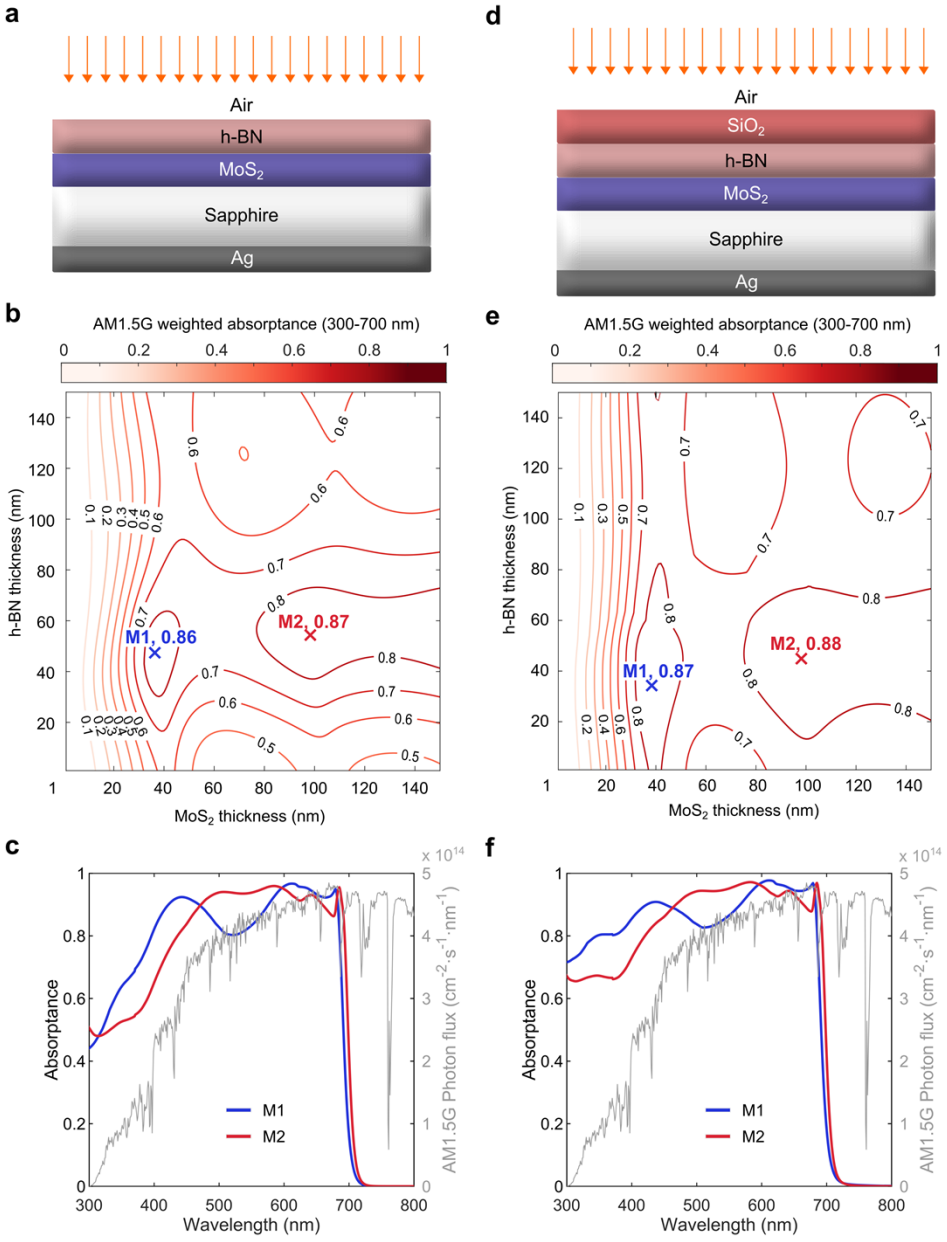

Fig. 5. (a) Schematic of h-BN/MoS_2/sapphire/Ag structure. (b) AM1.5G-weighted absorptance as a function of h-BN and MoS_2 thicknesses of structure in (a). (c) Spectral absorptance for the optimal cases of (b) M1 (blue) and M2 (red). (d) Same structure as in (a) with the addition of a SiO_2 top layer. (e) AM1.5G-weighted absorptance as a function of h-BN and MoS_2 thicknesses of structure in (d) for the optimal thickness of SiO_2. (f) Spectral absorptance for the optimal cases of (f) M1 (blue) and M2 (red). The optimized layer thicknesses and average absorptance for the curves in (c) and (f) can be found in Table 1.

Optics EXPRESS

this tuning of the absorptance spectrum through the addition of a second antireflective layer can be more important.

From Fig. 5 it can be concluded that the design containing a thick transparent substrate between the MoS_2 absorber and the metallic mirror equals the performance of the cavity only for MoS_2 thickness ≥ 30 nm. For thinner absorbers it is of interest only if it facilities the fabrication, improves the electrical properties, or reduces the cost. From a purely optical point of view, for very thin structures (zeroth FP order) the performance is worse than in the h-BN/MoS_2/Ag design, especially and the loss of interference effects cannot be redressed by improving antireflection with a double layer, at least for terrestrial applications. Interestingly, replacing Ag by Al as a low-cost option in the design with a thick transparent substrate does not produce a drastic reduction of the absorptance (see Supplementary Material, S5).

6. Absorptance of 1D cavities with double h-BN or ITO

We now consider a structure in which an ultrathin intermediate layer of h-BN is placed between the MoS_2 absorber and the metallic mirror, transforming the cavity shown in Fig. 4(d) into a quasi-symmetrical cavity as shown in Fig. 6(a). Figure 6(b) shows the AM1.5G-weighted absorptance contour map. The thickness of the bottom h-BN layer has been optimized at each point (see Supplementary Material, S8). In this cavity structure, the zeroth order maximum M0 is identical to the one found for the h-BN/MoS_2/Ag cavity, that is, 0.87 average absorptance and a maximum photocurrent density of 17.81 mA/cm^2 for 10 nm MoS_2 thickness. The thickness of the h-BN layers in this case are 31 nm (top) and 1 nm (bottom). Therefore, this structure makes it possible to encapsulate the MoS_2 absorber to improve back surface recombination while maintaining the zeroth order amplification. Furthermore, for non-optimal MoS_2 thicknesses around the M0 maximum, the cavity with a bottom h-BN layer exhibits a better performance. Very thin MoS_2 absorbers profit particularly from this architecture: a 4-nm-thick MoS_2 slab reaches 0.81 absorptance when embedded in an h-BN sandwich structure with a 1-nm-thick top layer and a 26-nm-thick bottom layer, whereas in the absence of a bottom layer it can only reach 0.59 for an optimized top h-BN layer of 32 nm. This makes the double h-BN cavity structure especially interesting if the technology is brought to the ultimate ultrathin limit.

We have seen that the introduction of thick transparent substrate between the MoS_2 and the mirror causes the M0 resonance to disappear (Fig. 5(b)). However, the introduction of a transparent ultrathin layer that places the absorber at nanometric distance of the mirror reinforces the resonance – it does not enhance the M0 maximum absorptance for an optimum MoS_2 thickness, but it broadens the M0 resonance peak. As demonstrated by Kats *et al.*,[25] when light impinges from a strongly absorbing medium (k of the order of n) onto a lossy metal, the reflection phase shift is not bound to be π and can, in principle, take any value. This allows a phase accumulation at the reflective interface, causing the resonance M0 at much smaller thicknesses than $\lambda/2n$. Our results show that adding a nanometric transparent layer between the absorber and the metal adds a new degree of freedom to tune the optical path of the interfering waves and maximize absorbance for sub-optimal absorber thickness. Janisch *et al* [47]. have shown a similar effect in a MoS_2 monolayer placed onto an Al substrate, reporting an increase in the absorption at $\lambda = 450$ nm from 0.23 to 0.67 if a 45-nm-thick Al_2O_3 layer is deposited between the monolayer and the metal.

The introduction of a bottom h-BN layer in the cavity has also an interesting effect on the M1 interference peak. The maximum absorbance becomes 0.89, the highest found among the structures studied here, with a maximum AM1.5G photocurrent density of 18.22 mA/cm^2. It is remarkable that M1 is attained with 57 nm of MoS_2 for a top and bottom h-BN layer of 52 nm and 48 nm, respectively. This means that the MoS_2 thickness at M1 can be reduced by ~40% in comparison to all previous cases while improving the absorptance. Additional calculations of a double h-BN cavity structure with an Al back-mirror have been performed and show similar

Optics EXPRESS

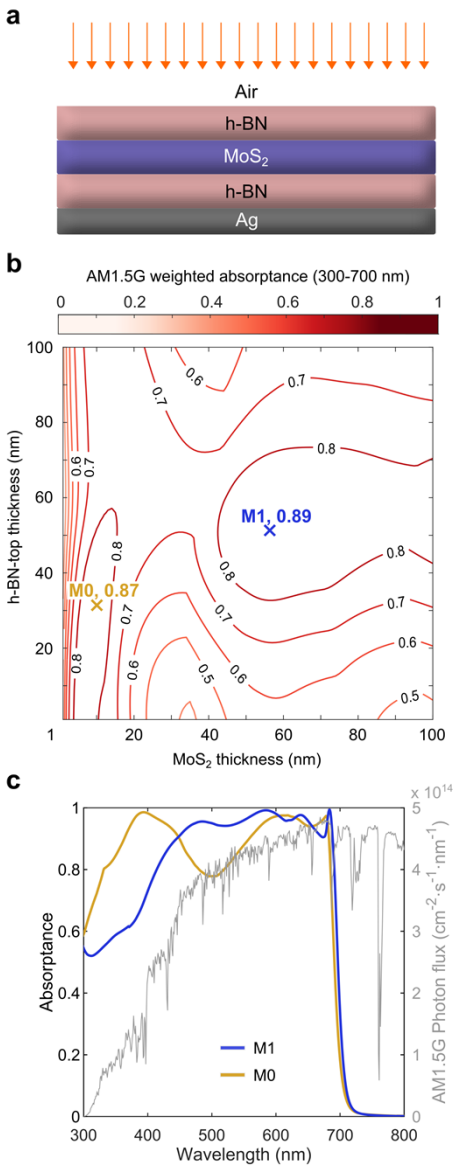

Fig. 6. (a) Schematic of h-BN/MoS_2/h-BN/Ag structure. (b) AM1.5G-weighted absorptance as a function of h-BN-top layer and MoS_2 thicknesses of structure in (a). The thickness of the h-BN-bottom layer has been optimized at each point in the map. (c) Spectral absorptance for optimal cases of (b) structure M0 (yellow) and M1 (blue). The optimum layer thicknesses and average absorptance for the curves in (c) can be found in Table 1.

values for the M1 resonance but a poorer performance at the M0 resonance. They can be found in the Supplementary Material, S9.

It is difficult to foresee at this point which maximum, M0 or M1, is more adequate for practical applications since the impact on the final device cost of a thickness reduction beyond 100 nm is unclear. For such extreme thinness, semiconductor material usage may have little influence on the final cost. It is possible to anticipate some indirect advantages and disadvantages of reducing the thickness to extreme values. For example, ultrathin devices with thickness ~ 10 nm will require a

Optics EXPRESS

shorter minority carrier diffusion length than a 100-nm-thick device. Therefore, it can be expected that the fabrication parameters can loosen up for extremely thin devices, which can lead to a reduction in cost (for example, the annealing time and temperature of solution-processed MoS_2 layers [31] could be reduced). On the other hand, having an extremely thin absorber increases the lateral series resistance and makes the fabrication of electrical contacts more demanding, which would probably lead to a more expensive processing.

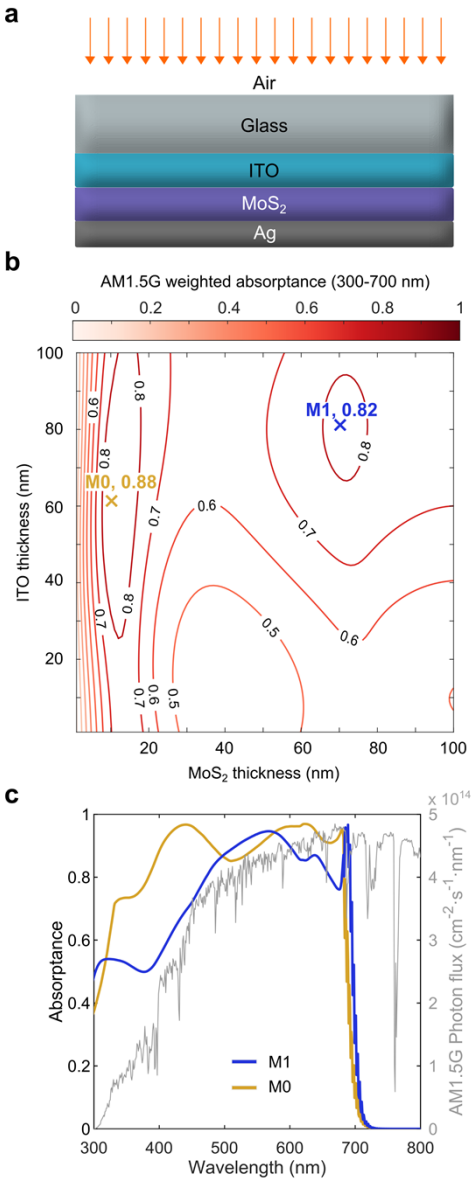

Fig. 7. (a) Schematic of glass/ITO/MoS_2/Ag structure. (b) AM1.5G-weighted absorptance map as a function of ITO and MoS_2 thicknesses of structures in (a). (c) Spectral absorptance for optimal cases of (b) M0 (yellow) and M1 (blue). The optimized layer thicknesses and average absorptance for the curves in (c) can be found in Table 1.

Optics EXPRESS

Figure 7 presents the last studied architecture. In this case the MoS_2 absorber is located between an on-glass ITO top contact and an optically thick Ag back contact. We consider this structure interesting because it resembles many stat-of-the-art low-cost photovoltaic devices based on organic or perovskite absorbers. Again, we have assumed that the MoS_2 absorber contains a pn junction and no hole and electron selective contact layers are needed. The results are encouraging because they show a remarkable M0 resonance with 0.88 average absorptance and a maximum photocurrent density of 18.01 mA/cm^2 for a MoS_2 thickness of 11 nm. This value is marginally superior to the one achieved with the h-BN cavities, while the M1 resonance is weaker (0.82). However, these results must be taken with caution because the practical roughness of the glass and ITO layer will determine to which extent the condition of coherence can be kept.

7. Comparison to other thin solar cells

Table 2 presents a compilation of experimental results reported for different solar cell technologies. In each case, a device has been chosen that is representative of the state of the art for very thin absorbers within that technology. The highest photocurrent density result obtained in this work for an ultrathin MoS_2 solar cell is also included: 18.2 mA/cm^2 for a 57-nm-thick absorber. This value is larger than the short-circuit current density produced by the flexible ultrathin device perovskite (thickness 350 nm). It is also comparable to the Si solar cell photocurrent density, although the band gap of Si is much narrower, and the Si absorber is 830 nm thick and is embedded in a nanophotonic structure. The CIGS and CdTe devices have moderately larger short-circuit currents density with absorbers that are 260 nm and 700 nm thick. Finally, the GaAs device exhibits a significantly higher photocurrent density of 24.6 mA/cm^2. Although in this case the GaAs absorber is 205 nm thick, the thickness of the complete epitaxial structure is 1.5 µm and the device includes a silver nanostructured back mirror, which makes the comparison to low-cost options difficult.

Table 2. Comparison between TMDC-based solar cells and other ultrathin solar cells

Technology	*Efficiency (%)*	*Short-circuit current density (mA/cm^{-2})*	*Absorber thickness (nm)*
Si [7]	8.6	19.7	830
GaAs [3]	19.9	24.6	205
CIGS [48]	8.1	21.0	360
CdTe [49]	11.2	21.7	700
Perovskite [50]	14	17.3	350
This work	-	18.2	57
		17.8	10

8. Conclusions

We have modelled the broadband absorption of ultrathin MoS_2-based solar cell structures, proposing several optical designs. We have demonstrated that just by adding an optimized top layer of h-BN - a layered material which is known to improve the surface properties of TMDCs - a 120 nm MoS_2 slab supported by a transparent substrate can absorb 84% of the photons contained in the 300-700 nm range of the AM1.5G spectrum. For a 1D cavity design containing a MoS_2 absorber as thin 10 nm, the average absorption in this spectral range reaches 87%. This is achieved by exploiting the zeroth-order Fabry-Perot resonance, amplifying it in a cavity containing an Ag reflector and one or two layers of h-BN. In future solar fabrication, a preferred cavity architecture can be chosen from the ones proposed here to match the MoS_2

Optics EXPRESS

thickness that optimizes the electronic performance of the device. For extremely thin MoS_2 slabs, between 1 and 9 nm thick, the h-BN/MoS_2/h-BN/Ag cavity gives the highest absorption, whereas from 10 nm on, a more compact h-BN/MoS_2/Ag cavity gives similar results. For absorbers ≥ 30 nm an h-BN/MoS_2/sapphire substrate/Ag architecture can also produce very high absorption. In all three structures a moderate MoS_2 thickness between 60 and 100 nm can also lead to ~90% average absorptance associated to the first-order Fabry-Perot resonance. We have further shown that it is possible to enhance the monochromatic absorption in 10-nm-thick MoS_2 to 0.98. Our results demonstrate that the light absorption of ultrathin solar cells based on nanometric TMDC absorbers can compete with established technology just with the aid of very simple 1D light-trapping structures.

Funding. European Regional Development Fund (RTI2018-096937-B-C21); Agencia Estatal de Investigación (RTI2018-096937-B-C21); Universidad Politécnica de Madrid (Programa Propio); Fundación Sener (Project SOUL); Fundación Ramón Areces (Project SuGaR).

Acknowledgments. The authors are grateful to Ignacio Tobías and Antonio Martí for fruitful discussions. This work has been partially supported by Fundación SENER within the research project SOUL, by grant RTI2018-096937-B-C21 funded by MCIN/AEI/10.13039/501100011033 and "ERDF A way of making Europe", and by Fundación Ramón Areces within the research project SuGaR. C.B-B is grateful to Universidad Politécnica de Madrid for funding through the Predoctoral Grant Programme (Programa Propio).

Disclosures. The authors declare that there are no conflicts of interest related to this article.

Data availability. The data that support the findings of this study are available on request from the corresponding author, EA.

Supplemental document. See Supplement 1 for supporting content.

References

1. I. Massiot, A. Cattoni, and S. Collin, "Progress and prospects for ultrathin solar cells," Nat. Energy **5**(12), 959–972 (2020).
2. M. Green, E. Dunlop, J. Hohl-Ebinger, M. Yoshita, N. Kopidakis, and X. Hao, "Solar cell efficiency tables (version 57)," Prog. Photovolt. Res. Appl. **29**(1), 3–15 (2021).
3. H.-L. Chen, A. Cattoni, R. De Lépinau, A. W. Walker, O. Höhn, D. Lackner, G. Siefer, M. Faustini, N. Vandamme, J. Goffard, B. Behaghel, C. Dupuis, N. Bardou, F. Dimroth, and S. Collin, "A 19.9%-efficient ultrathin solar cell based on a 205-nm-thick GaAs absorber and a silver nanostructured back mirror," Nat. Energy **4**(9), 761–767 (2019).
4. J. Buencuerpo, T. E. Saenz, M. Steger, M. Young, E. L. Warren, J. F. Geisz, M. A. Steiner, and A. C. Tamboli, "Efficient light-trapping in ultrathin GaAs solar cells using quasi-random photonic crystals," Nano Energy **96**, 107080 (2022).
5. V. Steenhoff, M. Theuring, M. Vehse, K. von Maydell, and C. Agert, "Ultrathin Resonant-Cavity-Enhanced Solar Cells with Amorphous Germanium Absorbers," Adv. Opt. Mater. **3**(2), 182–186 (2015).
6. L. Britnell, R. M. Ribeiro, A. Eckmann, R. Jalil, B. D. Belle, A. Mishchenko, Y.-J. Kim, R. V. Gorbachev, T. Georgiou, S. V. Morozov, A. N. Grigorenko, A. K. Geim, C. Casiraghi, A. H. C. Neto, and K. S. Novoselov, "Strong Light-Matter Interactions in Heterostructures of Atomically Thin Films," Science **340**(6138), 1311–1314 (2013).
7. V. Depauw, C. Trompoukis, I. Massiot, W. Chen, A. Dmitriev, P. R. i Cabarrocas, I. Gordon, and J. Poortmans, "Sunlight-thin nanophotonic monocrystalline silicon solar cells," Nano Futur. **1**(2), 021001 (2017).
8. A. K. Geim and I. V. Grigorieva, "Van der Waals heterostructures," Nature **499**(7459), 419–425 (2013).
9. W. M. Haynes, D. R. Lide, and T. J. Bruno, *Abundance of Elements in the Earth's Crust and in the Sea, CRC Handbook of Chemistry and Physics*, (Taylor & Francis group, CRC Press, 2016), **97**.
10. D. Jariwala, A. R. Davoyan, J. Wong, and H. A. Atwater, "Van der Waals Materials for Atomically-Thin Photovoltaics: Promise and Outlook," ACS Photonics **4**(12), 2962–2970 (2017).
11. C.-H. Lee, G.-H. Lee, A. M. van der Zande, W. Chen, Y. Li, M. Han, X. Cui, G. Arefe, C. Nuckolls, T. F. Heinz, J. Guo, J. Hone, and P. Kim, "Atomically thin p-n junctions with van der Waals heterointerfaces," Nat. Nanotechnol. **9**(9), 676–681 (2014).
12. M. M. Furchi, A. Pospischil, F. Libisch, J. Burgdörfer, and T. Mueller, "Photovoltaic effect in an electrically tunable van der Waals heterojunction," Nano Lett. **14**(8), 4785–4791 (2014).
13. M. M. Furchi, F. Höller, L. Dobusch, D. K. Polyushkin, S. Schuler, and T. Mueller, "Device physics of van der Waals heterojunction solar cells," npj 2D Mater. Appl. **2**(1), 3–7 (2018).
14. R. Frisenda, A. J. Molina-Mendoza, T. Mueller, A. Castellanos-Gomez, and H. S. J. van der Zant, "Atomically thin p–n junctions based on two-dimensional materials," Chem. Soc. Rev. **47**(9), 3339–3358 (2018).
15. S. Wi, H. Kim, M. Chen, H. Nam, L. J. Guo, E. Meyhofer, and X. Liang, "Enhancement of Photovoltaic Response in Multilayer MoS_2 Induced by Plasma Doping," ACS Nano **8**(5), 5270–5281 (2014).

Optics EXPRESS

16. D. Jariwala, A. R. Davoyan, G. Tagliabue, M. C. Sherrott, J. Wong, and H. A. Atwater, "Near-Unity Absorption in van der Waals Semiconductors for Ultrathin Optoelectronics," Nano Lett. **16**(9), 5482–5487 (2016).
17. A.-J. Cho, S. D. Namgung, H. Kim, and J.-Y. Kwon, "Electric and photovoltaic characteristics of a multi-layer ReS_2/$ReSe_2$ heterostructure," APL Mater. **5**(7), 076101 (2017).
18. J. Ahn, P. J. Jeon, S. R. A. Raza, A. Pezeshki, S.-W. Min, D. K. Hwang, and S. Im, "Transition metal dichalcogenide heterojunction PN diode toward ultimate photovoltaic benefits," 2D Mater. **3**(4), 045011 (2016).
19. S. Svatek, C. Bueno-Blanco, D.-Y. Lin, J. Kerfoot, C. Macías, M. H. Zehender, I. Tobías, P. García-Linares, T. Taniguchi, K. Watanabe, P. Beton, and E. Antolín, "High open-circuit voltage in transition metal dichalcogenide solar cells," Nano Energy **79**, 105427 (2021).
20. A. Daus, C. J. McClellan, K. Schauble, J. C. Costa, R. W. Grady, L. Petti, G. Cantarella, N. Münzenrieder, and E. Pop, "Aluminum oxide as a dielectric and passivation layer for (flexible) metal-oxide and 2D semiconductor devices," Proc. SPIE **11687**, 116871I (2021).
21. J. Wong, D. Jariwala, G. Tagliabue, K. Tat, A. R. Davoyan, M. C. Sherrott, and H. A. Atwater, "High Photovoltaic Quantum Efficiency in Ultrathin van der Waals Heterostructures," ACS Nano **11**(7), 7230–7240 (2017).
22. X. Liu, T. Galfsky, Z. Sun, F. Xia, E. Lin, Y.-H. Lee, S. Kéna-Cohen, and V. M. Menon, "Strong light–matter coupling in two-dimensional atomic crystals," Nat. Photonics **9**(1), 30–34 (2015).
23. S. Wu, S. Buckley, A. M. Jones, J. S. Ross, N. J. Ghimire, J. Yan, D. G. Mandrus, W. Yao, F. Hatami, J. Vučković, A. Majumdar, and X. Xu, "Control of two-dimensional excitonic light emission via photonic crystal," 2D Mater. **1**(1), 011001 (2014).
24. X. Gan, Y. Gao, K. Fai Mak, X. Yao, R.-J. Shiue, A. van der Zande, M. E. Trusheim, F. Hatami, T. F. Heinz, J. Hone, and D. Englund, "Controlling the spontaneous emission rate of monolayer MoS_2 in a photonic crystal nanocavity," Appl. Phys. Lett. **103**(18), 181119 (2013).
25. M. A. Kats, R. Blanchard, P. Genevet, and F. Capasso, "Nanometre optical coatings based on strong interference effects in highly absorbing media," Nat. Mater. **12**(1), 20–24 (2013).
26. A. R. Beal and H. P. Hughes, "Kramers-Kronig analysis of the reflectivity spectra of 2H-MoS_2, 2H-$MoSe_2$ and 2H-$MoTe_2$," J. Phys. C: Solid State Phys. **12**(5), 881–890 (1979).
27. L. J. Phillips, A. M. Rashed, R. E. Treharne, J. Kay, P. Yates, I. Z. Mitrovic, A. Weerakkody, S. Hall, and K. Durose, "Dispersion relation data for methylammonium lead triiodide perovskite deposited on a (100) silicon wafer using a two-step vapour-phase reaction process," Data Brief **5**, 926–928 (2015).
28. D. E. Aspnes and A. A. Studna, "Dielectric functions and optical parameters of Si, Ge, GaP, GaAs, GaSb, InP, InAs, and InSb from 1.5 to 6.0 eV," Phys. Rev. B **27**(2), 985–1009 (1983).
29. R. E. Treharne, A. Seymour-Pierce, K. Durose, K. Hutchings, S. Roncallo, and D. Lane, "Optical Design and Fabrication of Fully Sputtered CdTe/CdS Solar Cells," J. Phys.: Conf. Ser. **286**, 012038 (2011).
30. M. Gloeckler and J. R. Sites, "Band-gap grading in Cu(In,Ga)Se2 solar cells," J. Phys. Chem. Solids **66**(11), 1891–1894 (2005).
31. H. Yang, A. Giri, S. Moon, S. Shin, J.-M. Myoung, and U. Jeong, "Highly Scalable Synthesis of MoS_2 Thin Films with Precise Thickness Control via Polymer-Assisted Deposition," Chem. Mater. **29**(14), 5772–5776 (2017).
32. J. Suh, T.-E. Park, D.-Y. Lin, D. Fu, J. Park, H. J. Jung, Y. Chen, C. Ko, C. Jang, Y. Sun, R. Sinclair, J. Chang, S. Tongay, and J. Wu, "Doping against the Native Propensity of MoS_2: Degenerate Hole Doping by Cation Substitution," Nano Lett. **14**(12), 6976–6982 (2014).
33. I. H. Malitson, "Refraction and Dispersion of Synthetic Sapphire," J. Opt. Soc. Am. **52**(12), 1377–1379 (1962).
34. I. H. Malitson, "Interspecimen Comparison of the Refractive Index of Fused Silica," J. Opt. Soc. Am. **55**(10), 1205–1209 (1965).
35. G. Cappellini, G. Satta, M. Palummo, and G. Onida, "Optical properties of BN in cubic and layered hexagonal phases," Phys. Rev. B **64**(3), 035104 (2001).
36. M. J. Dodge, "Refractive properties of magnesium fluoride," Appl. Opt. **23**(12), 1980–1985 (1984).
37. B. Song, H. Gu, M. Fang, X. Chen, H. Jiang, R. Wang, T. Zhai, Y.-T. Ho, and S. Liu, "Layer-Dependent Dielectric Function of Wafer-Scale 2D MoS_2," Adv. Opt. Mater. **7**(2), 1801250 (2019).
38. D. Wickramaratne, L. Weston, and C. G. Van de Walle, "Monolayer to Bulk Properties of Hexagonal Boron Nitride," J. Phys. Chem. C **122**(44), 25524–25529 (2018).
39. G. A. Ermolaev, Y. V. Stebunov, A. A. Vyshnevyy, D. E. Tatarkin, D. I. Yakubovsky, S. M. Novikov, D. G. Baranov, T. Shegai, A. Y. Nikitin, A. V. Arsenin, and V. S. Volkov, "Broadband optical properties of monolayer and bulk MoS_2," npj 2D Mater. Appl. **4**(1), 21 (2020).
40. C. Hsu, R. Frisenda, R. Schmidt, A. Arora, S. M. Vasconcellos, R. Bratschitsch, H. S. J. Zant, and A. Castellanos-Gomez, "Thickness-Dependent Refractive Index of 1L, 2L, and 3L MoS_2, $MoSe_2$, WS_2, and WSe_2," Adv. Opt. Mater. **7**(13), 1900239 (2019).
41. E. Centurioni, "Generalized matrix method for calculation of internal light energy flux in mixed coherent and incoherent multilayers," Appl. Opt. **44**(35), 7532–7539 (2005).
42. J. Gusakova, X. Wang, L. Shiau, A. Krivosheeva, V. Shaposhnikov, V. Borisenko, V. Gusakov, and B. Tay, "Electronic Properties of Bulk and Monolayer TMDs: Theoretical Study Within DFT Framework (GVJ-2e Method)," Phys. Status Solidi A **214**(12), 1700218 (2017).
43. J. M. Llorens, J. Buencuerpo, and P. A. Postigo, "Absorption features of the zero frequency mode in an ultra-thin slab," Appl. Phys. Lett. **105**(23), 231115 (2014).

Optics EXPRESS

44. J. M. Llorens, J. Buencuerpo, J. M. Ripalda, and P. A. Postigo, "Amplification of the zeroth Order mode in ultra-thin layers," J. Green Eng. **5**(4), 71–82 (2016).
45. C. Yelgel, Ö. C. Yelgel, and O. Gülseren, "Structural and electronic properties of MoS_2, WS_2, and WS_2/MoS_2 heterostructures encapsulated with hexagonal boron nitride monolayers," J. Appl. Phys. **122**(6), 065303 (2017).
46. K. M. Islam, R. Synowicki, T. Ismael, I. Oguntoye, N. Grinalds, and M. D. Escarra, "In-Plane and Out-of-Plane Optical Properties of Monolayer, Few-Layer, and Thin-Film MoS_2 from 190 to 1700 nm and Their Application in Photonic Device Design," Adv. Photonics Res. **2**(5), 2000180 (2021).
47. C. Janisch, H. Song, C. Zhou, Z. Lin, A. L. Elías, D. Ji, M. Terrones, Q. Gan, and Z. Liu, "MoS_2 monolayers on nanocavities: enhancement in light–matter interaction," 2D Mater. **3**(2), 025017 (2016).
48. O. Lundberg, M. Bodegård, J. Malmström, and L. Stolt, "Influence of the Cu(In,Ga)Se2 thickness and Ga grading on solar cell performance," Prog. Photovolt. Res. Appl. **11**(2), 77–88 (2003).
49. A. Gupta, V. Parikh, and A. D. Compaan, "High efficiency ultra-thin sputtered CdTe solar cells," Sol. Energy Mater. Sol. Cells **90**(15), 2263–2271 (2006).
50. Y. Li, L. Meng, Y. Michael Yang, G. Xu, Z. Hong, Q. Chen, J. You, G. Li, Y. Yang, and Y. Li, "High-efficiency robust perovskite solar cells on ultrathin flexible substrates," Nat. Commun. **7**(1), 10214 (2016).